Study on Shadow Detection of World View-II Remote Sensing Image Based on Band Standardization

Junwei Xin[1], Xiaoyong Chen[1], Zixin Liu[1], Yan Luo[1], Zhenxing Liu[2]*

[1] State Key Laboratory of Nuclear Resources and Environment, East China University of Technology, China
[2] School of Information Engineering, East China University of Technology, China
xinjunwei@ecut.edu.cn, 200960002@ecut.edu.cn, paololew@ecut.edu.cn, yanluo@ecut.edu.cn, 200260015@ecut.edu.cn

Abstract

This paper presents a valid shadow detection method subjected to WorldView-II remote images combining band standardization with principal component transformation algorithm. Eight bands among The WorldView-II image, each band indicates a specified range of values. Firstly, each band is standardized to the same scale, then utilizing three optimal bands forms a new single band. According to the characteristics of principal component, if the gray value of dark material is positive, just take it for granted, which will be used in next operation. Once the gray value is negative, it will be inverted comparing with the former. In this study, selecting the above adaption builds up an advanced shadow index. Experimental results show that the shadow index can distinguish the shadow from other objects effectively, such as water in high brightness, vegetation, roads, buildings. Meanwhile, there is no significant difference between the water in low brightness and high when using the shadow index. To cope with this problem, we propose an advanced water index based on the normalized differential water index, which is constructed to eliminate the interference of water in low brightness. Results indicate that the indexes can accurately distinguish shadow regions in the WorldView-II image data.

Keywords: Shadow detection, Remote sensing, Band standardization, Shadow indexes

1 Introduction

WorldView-II remote sensing image data is one of the new generations of high-resolution satellite images at the centimeter level. Worldview-II has eight bands, its higher resolution and rich multi-spectral bands are more conducive to extract valid information, accurately detect changes and easily map. However, due to the existence of shadows, image classification and feature recognition of WorldView-II remote sensing images are extremely difficult. Therefore, accurately detecting and eliminating the shadow region has become a research hotspot [1-2]. Shadow detection methods are mainly based on models or shadow attributes [3]. Model-based methods which often require too many prior conditions, which means large limitations. Detection methods based on shadow attributes have strong applicability, most of which extract shadows based on geometric and spectral characteristics of shadows [4-5]. According to the characteristics of the first principal component of the shadow, Liu et al. [6] proposed a detection method based on principal component analysis (PCA) and Hue-Intensity-Saturation (HIS) transformation. Yang et al. [7] used principal component transformation and calculation of bands to highlight the shadow information in their research on the ZY-3 satellite image. Liu et al. [8] corrected the radiance of shadow area to the same level as that of shadow free areas, and then used an object-based classification method to detect building areas and produced a shadow-free image by utilizing a linear function. Xie et al. [9] proposed an objected-oriented building shadow extraction method which integrates the image characteristic components and the shadow's morphological characteristics of buildings. The above methods were all aimed at remote sensing images with a small number of wavebands and could accurately detect the shadow under the corresponding conditions. However, there were still some problems in the results, such as interference information and inability to accurately distinguish water with shadow.

Based on the existing shadow detection methods, this paper proposes a shadow detection method suitable for Worldview-II image. In this study, the mean value and standard deviations are used to standardize eight bands, and all bands are put on the same scale. Then, the three bands with obvious feature differences are accumulated into obtaining a new single band. By using the new band, the feature of shadow is significantly different from other features as desired. Finally, combining the characteristics with the principal component transformation, an advanced method of shadow detection is proposed based on the principle of ratio type index. At the same time, combined with the characteristics of Worldview-II image, a new water index is proposed to eliminate water interference.

2 Spectral Characteristic Analysis and Band Standardization

The Worldview-II satellite is one of the remote sensing satellites with the most abundant spectral bands in the world. It can provide one panchromatic band with ground

*Corresponding Author: Junwei Xin; E-mail: xinjunwei@ecut.edu.cn
DOI: 10.53106/160792642023052403003

resolution of 0.5 m and 8 bands of multi-spectral image data with ground resolution of 1.8 m respectively, among which the multi-spectral data are CB (Coastal Blue), B (Blue), G (Green), Y (Yellow), R (Red), Re (Red edge), NIR_1 (Near Infrared 1) and NIR_2 (Near Infrared 2). In the study area of this paper, we first fused the panchromatic image of 0.5 m with the multispectral image of 1 m. Then we selected five typical features such as shadow, water, road, building and vegetation from the 0.5 m fusion image, and their spectral information was counted to obtain the change curve of Digital Number (DN) value (Figure 1). Table 1 provides the descriptive statistics of the extracted features.

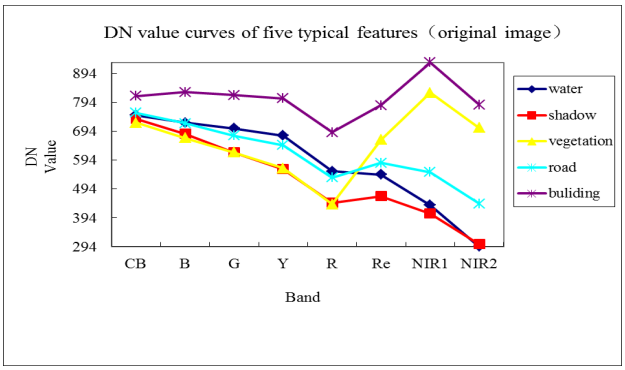

Figure 1. DN value curves of five typical features

Table 1. The statistical values of shadow and other extracted features

	Water		Shadow		Vegetation		Road		Building	
Band	Mean	Standard deviation	Mean	Standard deviation	Mean	Standard deviation	Mean	Standard deviation	Mean	Standard deviation
CB	749.4	7.48	736.1	14.54	723.2	22.62	758.1	19.01	816.8	73.07
B	723.5	8.07	685.4	18.88	670.5	22.01	721.3	19.85	829.3	117.36
G	703.8	13.44	620.8	26.58	620.2	31.38	679.0	27.08	819.1	151.24
Y	679.1	20.94	562.9	30.06	565.4	36.47	645.1	32.30	807.5	195.10
Re	555.6	21.42	446.0	28.94	441.2	29.13	533.0	32.17	690.6	191.51
R	544.2	19.13	469.3	32.07	664.8	119.50	584.3	41.74	783.3	232.48
NIR_1	438.3	12.21	408.3	36.94	827.0	218.39	552.0	51.36	932.0	300.28
NIR_2	294.4	6.9	302.7	27.52	706.6	208.78	443.4	46.29	786.8	254.86

As we can see in Table 1, the mean values of shadow, water and vegetation were close to each other and indistinguishable in the visible light range. But in the NIR_1 and NIR_2 bands, the gray value of shadow and water dropped sharply compared with other features. Moreover, mean values of the extracted five features differed greatly in different wavebands coupled with different range of values. For better comparative analysis, we use equation (1) to standardize all bands by utilizing the mean and standard deviation values (Table 1), where $G(i, j)$ express initial image, μ_i means the mean, and σ_i depicts standard deviation.

$$band_i^* = \frac{G(i,j) - \mu_i}{\sigma_i}. \quad (1)$$

Then the data of all bands were standardized to the same scale. After calculating the gray level information of the five features in the original 8 bands and the standardized eight bands, we obtained the gray level curves of each feature, as shown in Figure 1 and Figure 2.

As for Figure 1 and Figure 2, in the original band, the variation trends of water and shadow were consistent and closely in the whole band range, so it is difficult to distinguish them. In the visible light range, the distinction between shadow, water, road, and vegetation was not obvious, while in the NIR_1 and NIR_2, vegetation, road and buildings were higher than water and shadow. After standardization, the shadow was negative in the whole band range, while the water was positive in the visible bands and negative in the range of near infrared band and red edge band. The shadow was clearly distinguished from water and buildings, and the spectral curves of the shadow and vegetation were consistent in the visible bands range, but significantly lower than vegetation in the NIR_1 and NIR_2 band. But in the NIR_2 band, the gray value of water and shadow was so close to each other.

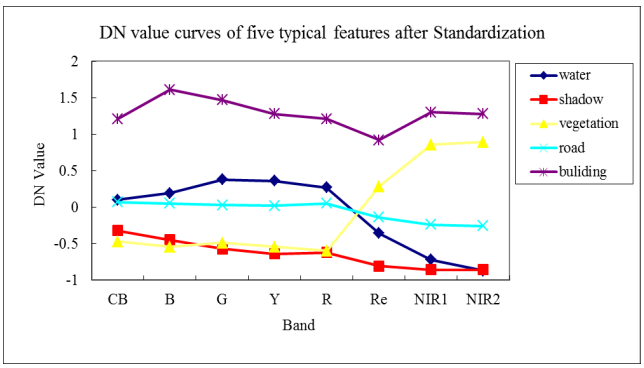

Figure 2. DN value curves of five typical features after standardization

Table 2. Gray scale statistics of shadow and four other typical features

Typical features	Min value	Max value	Mean value	
Water	-1.39	0.71	0.01	
Shadow	-2.99	0.17	-2.07	
Vegetable	-2.36	3.98	-0.18	B_{347}^*
Road	-1.84	2.10	-0.18	
Building	-1.26	12.22	4.04	
Water	-1.46	0.62	-0.07	
Shadow	-3.03	0.39	-1.94	
Vegetable	-2.31	3.45	-0.23	B_{357}^*
Road	-1.76	2.08	-0.16	
Building	-1.19	12.41	3.98	
Water	-1.51	0.44	-0.22	
Shadow	**-2.95**	**-0.01**	**-1.94**	
Vegetable	-2.31	3.62	-0.19	B_{358}^*
Road	-1.72	2.11	-0.19	
Building	-1.15	11.99	3.96	
Typical features	Min value	Max value	Mean value	
Water	-1.39	0.71	0.01	
Shadow	-2.99	0.17	-2.07	
Vegetable	-2.36	3.98	-0.18	B_{347}^*
Road	-1.84	2.10	-0.18	
Building	-1.26	12.22	4.04	
Water	-1.46	0.62	-0.07	
Shadow	-3.03	0.39	-1.94	
Vegetable	-2.31	3.45	-0.23	B_{357}^*
Road	-1.76	2.08	-0.16	
Building	-1.19	12.41	3.98	
Water	-1.51	0.44	-0.22	B_{358}^*
Shadow	**-2.95**	**-0.01**	**-1.94**	
Vegetable	-2.31	3.62	-0.19	
Road	-1.72	2.11	-0.19	
Building	-1.15	11.99	3.96	

To sum up, the shadow was different from other corresponding ground objects in the 3, 4, 5, 7 and 8 bands, and we can obtain B_{347}*, B_{357}* and B_{358}* by band accumulation. The DN statistics of five typical features in these bands were also calculated, and the statistical results are shown in Table 2.

It can be seen from Table 2 that in these three combinations, the gray value of buildings is the largest, while the gray value of shadow, water and vegetation are relatively lower. It is also evident that the gray value of shadow was smaller than that of water. Comparison from the mean, minimum or maximum values (Table 2), the shadows in B_{358}* were all negative, but in B_{347}* and B_{357}* positive and negative values were obtained. By removing the features of positive value and retaining the features of negative value, the shadow and water would be separated from other features.

3 PCA Transform

Principal component analysis (PCA) is a linear transformation based on image statistics, which can reduce data redundancy and enhance its contrast, thus improving the accuracy of image segmentation and data extraction. Through PCA transformation, relevant multidimensional data can be compressed and separated into several independent bands [6]. After PCA transformation of the original WorldView-II satellite image, the variance contribution rate of the first principal component (PC_1) was above 95.08%. This implies that PC_1 can represent information of the original image by 95.08%. And in the histogram of PC_1, the dark materials, such as shadows and water, are generally located at either ends, negative small value end or large value end [6].

In Figure 3, the blue, red, green, black, and yellow curves represent the histograms of water, shadows, roads, buildings and vegetation, respectively. It can be seen that the water (blue curve) and the shadow (red curve) are both negative and located at the largest end of the negative value, while other ground objects have positive and negative gray values (see Figure 3). This indicates that the proportion of dark matter in this study area is small. By inverting PC_1, the shadow region value is located at the large end of PC_1.

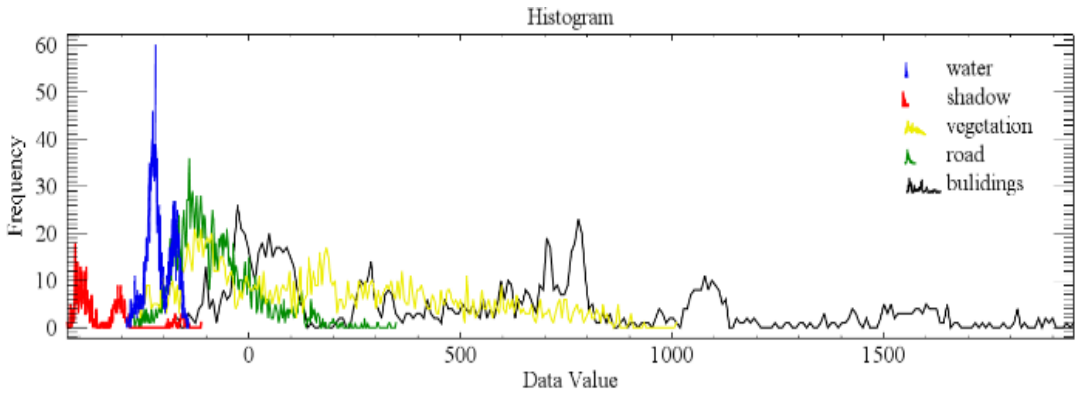

Figure 3. Histograms of shadows and four other typical features in PC_1 element

4 Variables Index

4.1 Shadow Index

Considering the above analysis, we constructed a new shadow index based on the principle of ratio type index to widen the gap between shadow features and other features [10]. Formula (2) describes the new shadow index

$$SI^* = PC_1^* \cdot \frac{|-B^*|}{NIR}. \tag{2}$$

Where SI^* is the new shadow index. $|-B^*|$ is the new band which has been regenerated after band standardization and NIR is the infrared band of the image. In applying Equation 2, the following were considered: when the shadow is located at the negative small value end, then PC_1^* is the opposite of PC_1; and if the shadow is located at the large value end of PC_1, then PC_1^* is equal to PC_1. After the SI^* transformation, the gray value of the shadow is differ from other features and water in high brightness, but still close to the gray value of some parts of the water in low brightness.

4.2 Water Index

The traditional water index is the ratio using the blue band and the Near-Infrared band of the image, due to the difference of gray value of water in green band and Near Infrared band is large [11], and Normalized Difference Water Index (NDWI) was built by S. K. Mcfeeters [12].

The WorldView-II satellite image has two Near Infrared bands (NIR_1 and NIR_2), and it could be seen from Figure 1 that the gray of water in the two Near-Infrared bands is the lowest in the whole band range, and the gray of NIR_2 is lower than the one of NIR_1.

Compared to other features, the minus of gray value of the three bands (Green, NIR_1 and NIR_2) is smaller and the sum of the same three bands is larger. The ratio using the minus and the sum above can be easier to detect the water information.

So, we developed a new water index ($NDWI^*$) capable of imitating $NDWI$ to detect water information, which is expressed in formula (3).

$$NDWI^* = \frac{2G - NIR_1 - NIR_2}{G + NIR_1 + NIR_2}. \tag{3}$$

In Equation 3, G, NIR_1 and NIR_2 respectively represent green band, Near-Infrared band 1 and Near-Infrared band 2 found in WorldView-II satellite image.

5 Experiments and Analysis

5.1 Shadow Detection Method Process

The technical process of the shadow detection model established in this paper is summarized in Figure 4.

By utilizing the mean and standard deviation values of the data, eight bands of the original image were standardized to the same scale. Then based on the spectral characteristics of the five selected features (water, vegetation, building, shadow, and road), we selected the best three bands for band accumulation to form a new single band, as shown in Equation 1.

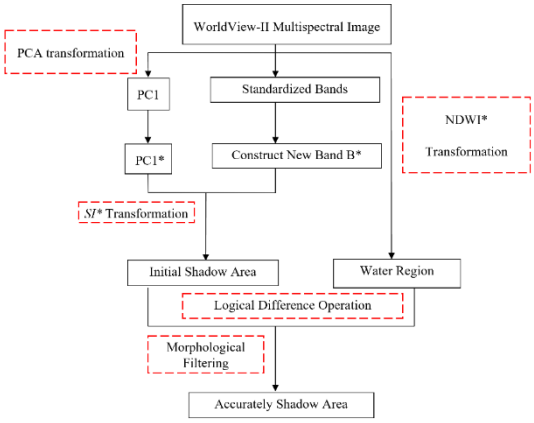

Figure 4. Flowchart of shadow detection algorithm

According to the characteristics of matter in dark color at both ends of the first principal component, the original image was performed with PCA transformation to extract the first principal component PC_1. Analysis of the histogram (Figure 3) showed that the shadow regions were located at the negative small value end in the PC_1. Here, $PC_1^* = -PC_1$, that is, reserving itself. At this point, the gray values of the shadow regions were at the largest positive end, followed by water. For the other features (building, road, and vegetation) their gray values were all smaller than the shadow.

The original image was transformed by the SI^* transformation method, and then we used threshold method to obtain initial shadow area. However, due to the similarity between water in low brightness and shadow region, initial shadow area was mixed with water in low brightness area.

We used the proposed $NDWI^*$ method we developed to transform the original image and extracted the water information in the original image by using the threshold method.

Based on the preliminary shadow regions obtained in step 3 and water information obtained in step 4, the logical difference operation was performed between them to obtain the shadow pattern spot information. Finally, we could obtain the final shadow region by a morphological filtering algorithm.

5.2 Shadow Index

To verify the accuracy of the proposed method, we first compared the shadow detection method with the Normalized Difference Umbra Index (NDUI) method, and then the water detection method with the Normalized Differential Water Index (NDWI) transformation. The shadow region was represented by white and the rest by black in the results.

In this paper, we selected four areas (A, B, C and D), which mainly include water, shadows, roads, buildings, and vegetation, to ascertain the effectiveness of the proposed method. From the analysis carried out, and the water and

shadow were so close to each other in NIR2 (Figure 1), we used the newly constructed B_{358}*, PC_1^* and NIR_1 to treat the study area by using equation 2. The threshold method was then used to segment the SI^* transformation image to obtain the preliminary shadow region as shown in Figure 5.

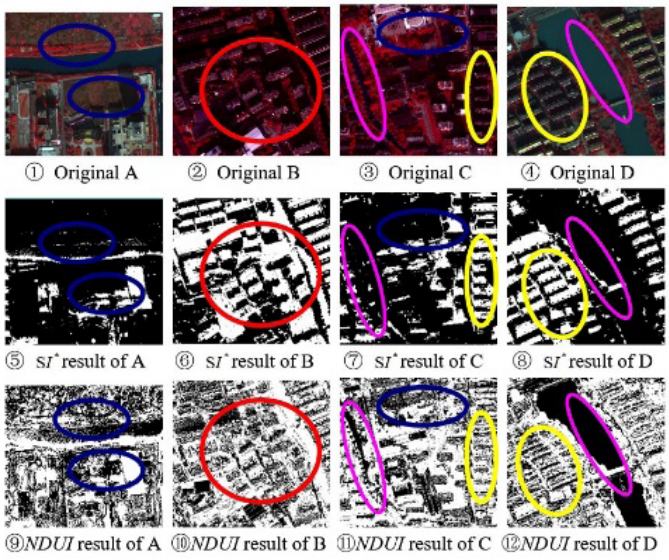

Figure 5. Comparison of initial shadow detection results in each experimental area

As can be seen from Figure 5, both the SI^* method and NDUI method can extract most of the shadows, while some water in high brightness can also be removed well, such as the water represented by the purple notes in areas C and D. However, by comparison, it can be found that the vegetations near the water in area C and D have been confused into shadow in the NDUI method, in addition to the vegetations near the river in area A and the woods near the square in area C (blue circle note). But the SI* method can eliminate them well. In some other densely populated areas, such as areas B, C and D, where red circles are indicated, the shadow information can be obtained well, and the shadow boundaries are clear and distinct. While in the NDUI method, the boundaries between the outlines of the house and the shadow area are indistinct. Therefore, it can be seen that the SI^* method is better than the NDUI method in extracting shadows from vegetation areas and densely populated areas.

However, there is still some water information interference, such as water in low brightness in zone A and B. To get rid of water information confused in the shadow area effectively, we used the $NDWI^*$ method to transform the original image, and segmented water final by the threshold value method. To verify the effect, the results were compared with the results of NDWI transform as shown in Figure 6(a) to Figure 6(f).

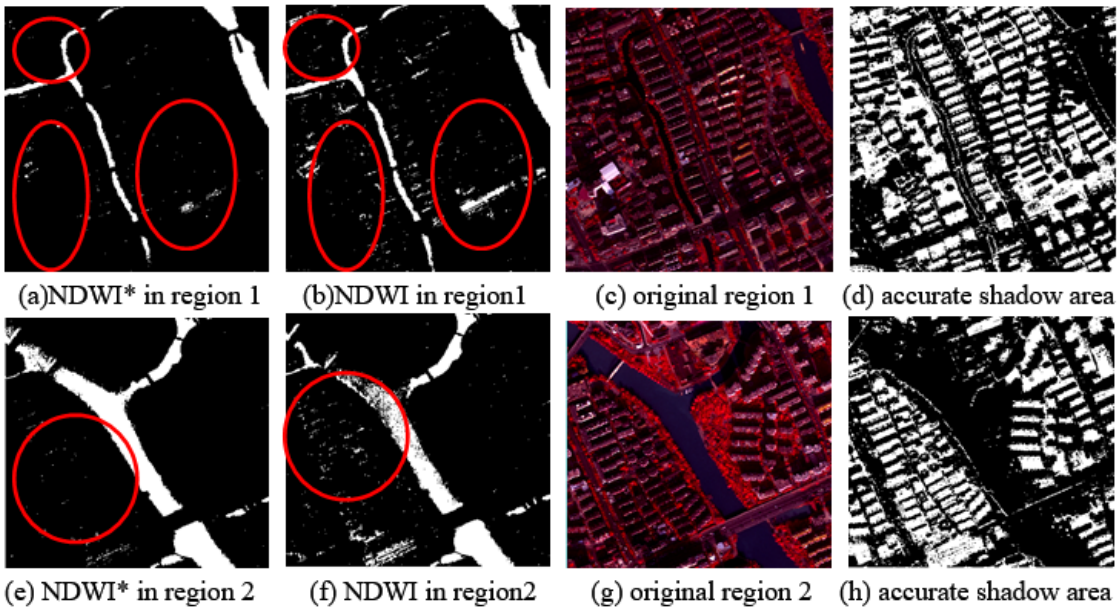

Figure 6. Comparison of water extraction and accurate shadow detection results

In Figure 6(a) to Figure 6(f), water information has been better separated and extracted in the $NDWI^*$ method and the NDWI method. However, it is obvious that some parts of the shadow information in the NDWI method are confused into water (see red circles in Figure 6). The gray values of the transformation results of water and shadow in the NDWI method and the $NDWI^*$ are calculated, as shown in Table 3.

Table 3. Statistical comparison of water and shadow

	NDWI		*NDWI**	
Feature	Min value	Max value	Min value	Max value
River	0.210851	0.248227	0.299069	0.330838
Shadow	0.145581	0.237895	0.209515	0.298203

As can be seen from Table 3, the minimum gray value of water (0.210851) is so close to the maximum gray value of shadows 0.237895 by the NDWI method. Meanwhile in the result of $NDWI^*$ transformation, the minimum gray value of water is 0.299069 and the maximum gray value of shadows is 0.298203. There is a clear spacing between water and shadow. It is shown that comparing with NDWI method, the new water index $NDWI^*$ can be better to extract water information from the original image.

Finally, by using the water area extracted by the NDWI* method and initial shadow regions obtained by method, we can obtain the final accurate shadow regions by the logical non-operation, as shown in Figure 6.

According to the accurate shadow detection results as shown in Figure 6(d) and Figure 6(h), the water information extracted by the $NDWI^*$ method has been well segmented from the initial shadow detection and the final accurate shadow areas have been obtained.

Through the above qualitative analysis, the method combined with the $NDWI^*$ method proposed in this paper has much more advantages than the traditional detection method in the aspect of shadow detection. To analyse the accuracy of the algorithm more objectively, the results are compared and judged quantitatively [13]. The proposed method, the traditional NDUI threshold method (combined with NDWI method) and the manual interpretation method are compared and analysed, and statistics are made for the two experimental areas to calculate the correct detection rate and missing rate of pixels. The statistical results are shown in Table 4.

As can be seen from Table 4, the extraction accuracies of the proposed method for these two regions are 90.02% and 91.73%, respectively, which are significantly better than the ones of the traditional NDUI detection method. Moreover, the effect of shadow detection is better.

Table 4. Accuracy evaluation of shadow detection results

	$SI^* + NDWI^*$ (pixels)	$NDUI + NDWI$ (pixels)	Manual acquisition (pixels)	Correct extraction ratio %		Leakage rate % ($SI^* + NDWI^*$)
				$SI^* + NDWI^*$	$NDUI + NDWI$	
Region 1	779744	1219640	866189	90.02	71.02	5.07
Region 2	471488	633976	513995	91.73	74.37	4.78

6 Conclusion

Generally, the shadow area is easily confused with water. We proposed an efficient shadow detection method, which is suitable for multi-band image, to solve such scenario. According to the characteristics of World View-II image, a fresh shadow index is constructed by combining band standardization and principal component transformation. Experimental results show that the method can segment shadow from water in high brightness and other features effectively. To eliminate the water in low brightness, a new water index $NDWI^*$ is generated to get the water information from the original image. As a result, the accurate shadow region after the logical difference operation and morphological operation can be obtained.

Acknowledgment

This work is supported by The National Natural Science Foundation of China (Nos. 41861062), Scale-Span Low-Altitude and Spaceborne High-Resolution Multi-Source Remote Sensing Images Intelligent Registration and Fusion.

References

[1] K. K. Singh, K. Pal, M. Nigam, Shadow detection and removal from remote sensing images using ndi and morphological operators, *International journal of computer applications*, Vol. 42, No. 10, pp. 37-40, March, 2012.

[2] Y. Chen, D. Wen, L. Jing, P. Shi, Shadow information recovery in urban areas from very high resolution satellite imagery, *International Journal of Remote Sensing*, Vol. 28, No. 15, pp. 3249-3254, July, 2007.

[3] V. Ar´evalo, J. Gonz´alez, G. Ambrosio, Shadow detection in colour high-resolution satellite images, *International Journal of Remote Sensing*, Vol. 29, No. 7, pp. 1945-1963, April, 2008.

[4] H. Luo, L. Wang, Z. Shao, D. Li, Development of a multi-scale object-based shadow detection method for high spatial resolution image, *Remote Sensing Letters*, Vol. 6, No. 1, pp. 59-68, January, 2015.

[5] N. Tatar, M. Saadatseresht, H. Arefi, A. Hadavand, A robust object-based shadow detection method for cloud-free high resolution satellite images over urban areas and water bodies, *Advances in Space Research*, Vol. 61, No. 11, pp. 2787-2800, June, 2018.

[6] H. Liu, T. Xu, Study on shadow detection in high resolution remote sensing image of PCA and HIS model, *Remote Sensing Technology and Application*, Vol. 28, No. 1, pp. 78-84, February, 2013.

[7] X. Yang, S. Yang, Z. Liu, H. Yao, Y. Li, Shadow detection for urban tall standing objects based on ZY-3 satellite imagery, *Science of Surveying and Mapping*, Vol. 40, No. 9, pp. 98-101, September, 2015.

[8] W. Liu, F. Yamazaki, Object-based shadow extraction and correction of high-resolution optical satellite images, *IEEE Journal of Selected Topics in Applied*

Earth Observations and Remote Sensing, Vol. 5, No. 4, pp. 1296-1302, August, 2012.
[9] Y. Xie, D. Feng, Q. Li, Y. Wang, M. Hu, Building shadow detection with integrated characteristic components for high resolution remote sensing images, *Bulletin of Surveying and Mapping*, No. 10, pp. 61-65, October, 2018.
[10] J. Shen, L. Yang, X. Chen, J. Li, Q. Peng, J. Hu, A method for object-oriented automatic extraction of lakes in the mountain area from remote sensing image, *Remote Sensing for Land & Resources*, Vol. 24, No. 3, pp. 84-91, September, 2012.
[11] H. Xu, A study on information extraction of water body with the modified normalized difference water index (mndwi), *Journal of Remote Sensing-Beijing*, Vol. 9, No. 5, pp. 589-595, September, 2005.
[12] S. K. McFeeters, The use of the normalized difference water index (ndwi) in the delineation of open water features, *International journal of remote sensing*, Vol. 17, No. 7, pp. 1425-1432, May, 1996.
[13] Q. Li, D. Feng, M. Hu, Y. Wu, L. Yang, Shadow detection of integrated characteristic components for gf-2 image, *Remote Sensing Technology and Application*, Vol. 34, No. 6, pp. 1252-1260, December, 2019.

Biographies

Junwei Xin, Male, born in April 1987, is a doctoral candidate in geological resources and geological engineering of East China University of Technology, mainly engaged in the research on the integration of deep learning methods and geological remote sensing technology.

Xiaoyong Chen, Male, born in September 1961, professor, doctor, doctoral supervisor, mainly engaged in theoretical research and application technology development of geographic information science.

Zixin Liu, male, born in 1985, lecturer at East China University of Technology, majoring in software engineering. Engaged in the research of hardware Side-channel attack, artificial intelligence, and digital geological crossover application.

Yan Luo, Female, born in October 1983, university lecturer, master, teacher of East China University of Technology, mainly engaged in the research of photogrammetry technology and remote sensing image processing methods.

Zhenxing Liu, Male, born in April 1984, is a doctoral candidate in geological resources and geological engineering of East China University of Technology, mainly engaged in the research on the 3D geological intelligent modeling.